Faraday Discussions
Cite this: *Faraday Discuss.*, 2024, **251**, 140



PAPER



# Transient IR spectroscopy of optically centrifuged $CO_2$ (R186–R282) and collision dynamics for the $J = 244$–$282$ states

Michael E. Ritter, Simone A. DeSouza, Hannah M. Ogden, Tara J. Michael and Amy S. Mullin *

Received 20th December 2023, Accepted 4th April 2024
DOI: 10.1039/d3fd00179b

Collisions of optically centrifuged $CO_2$ molecules with $J = 244$–$282$ ($E_{rot} = 22\,800$–$30\,300$ cm$^{-1}$) are investigated with high-resolution transient IR absorption spectroscopy to reveal collisional and orientational phenomena of molecules with hyper-thermal rotational energies. The optical centrifuge is a non-resonant optical excitation technique that uses ultrafast, 800 nm chirped pulses to drive molecules to extreme rotational states through sequential Raman transitions. The extent of rotational excitation is controlled by tuning the optical bandwidth of the excitation pulses. Frequencies of 30 R-branch $\nu_3$ fundamental IR probe transitions are measured for the $J = 186$–$282$ states of $CO_2$, expanding beyond previously reported IR transitions up to $J = 128$. The optically centrifuged molecules have oriented angular momentum and unidirectional rotation. Polarization-sensitive transient IR absorption of individual rotational states of optically centrifuged molecules and their collision products reveals information about collisional energy transfer, relaxation kinetics, and dynamics of rotation-to-translation energy transfer. The transient IR probe also measures the extent of polarization anisotropy. Rotational energy transfer for lower energy molecules is discussed in terms of statistical models and a comparison highlights the role of increasing energy gap with $J$ and angular momentum of the optically centrifuged molecules.

## I. Introduction

Molecules in high energy rotational states are observed in plasmas, as products of photodissociation and collisional energy transfer, and in exoplanet atmospheres, yet much remains to be understood about their behavior and properties.[1–8] Of particular interest here is the collisional energy transfer behavior of molecules with large amounts of rotational energy. Linear molecules have rotational energies that increase essentially as the square of the rotational quantum number $J$,

*Department of Chemistry and Biochemistry, University of Maryland College Park, College Park, Maryland 20742, USA. E-mail: mullin@umd.edu*

 

leading to increasing energy gaps between states as a function of $J^2$. The role of energy gaps in statistical models of energy transfer of low energy molecules is well established, but we are yet to understand how large rotational energy gaps affect collisional energy transfer.[9]

High energy rotational states of molecules cannot be populated using traditional optical approaches because selection rules for absorption and Raman processes limit changes in the rotational angular momentum to small $\Delta J$ values. Recent advances in optical control of molecular rotation have led to new methods for controlling alignment, orientation, energy and directionality of molecular rotors.[10–50] These techniques include using a pair of orthogonally polarized pulses of light with a time delay, a sequence of pulse trains with varying pulse lengths, and a pair of oppositely chirped pulses. The first two techniques can control a component of molecular motion but are limited to relatively low-$J$ states.[10–15] The third technique is the optical centrifuge which can prepare molecules in extreme rotational states and has been used to investigate the properties and dynamics for a number of systems.[16–50]

In the work reported here, we use a tunable optical centrifuge to prepare rotationally excited $CO_2$ molecules and investigate their collision dynamics using high-resolution transient IR absorption spectroscopy. The collision studies focus on $CO_2$ with $J = 244$–$282$ and rotational energies of $E_{rot} = 22\,800$–$30\,300$ cm$^{-1}$. To perform these studies, we first used high-resolution transient IR absorption spectroscopy to identify line-center frequencies of 30 R-branch transitions with $J = 186$–$282$ of the $CO_2$ $\nu_3$ fundamental absorption band and then used the IR transitions to investigate the collision dynamics of the optically centrifuged $CO_2$ molecules.

Previously, high-resolution IR transitions for $CO_2$ have been reported up to $J = 128$ in the HITRAN database.[51,52] Transitions up to $J = 146$ have also been observed in dispersed IR emission from a flame, but populating high-$J$ states by thermal heating leads to spectral broadening and congestion, making identification of state-resolved transition frequencies difficult.[1] The HITEMP database reports transitions up to $J = 200$ based on semi-empirical calculations.[53] The Carbon Dioxide Spectral Database at 4000 K (CDSD4000) reports IR absorption transitions for $CO_2$ at 4000 K based on effective Hamiltonian calculations that include 41 vibrational states and 300 rotational states.[54] For the IR transitions reported here, we used a combination of a third-order expansion of the rigid rotor model and the CDSD4000 as a guide for identifying the $CO_2$ transition frequencies.

Spectral lines of high rotational states of $CO_2$ are used to study combustion processes, and the atmospheres of Venus and exoplanets.[5–8,55–57] These studies have relied on calculated transition frequencies to identify the high-$J$ $CO_2$ states. The new high-$J$ transition frequencies reported here will serve as benchmark for future spectral calculations and databases.[54,58]

Previously, we have investigated collisions of optically centrifuged $CO_2$ by probing P-branch transitions for states with $J < 104$.[18,20,21,23,24] In the first of these studies in 2011, single-pass IR detection was used to investigate the collision dynamics of centrifuged $CO_2$ molecules with $62 \leq J \leq 88$.[18] With the single-pass IR detection, a polarization-sensitive study of the $J = 76$ state of $CO_2$ showed that even after 1000 collisions, there was a preference for population to remain in the original plane of rotation.[20] In 2015, a $J$-dependent survey of $CO_2$ states $0 \leq J \leq 100$

showed that collisions of centrifuged molecules preferentially involve a translationally cool subset of molecules from the low-$J$ states.[21] This study measured large translational energies for states with $J = 36$–$100$ that result from collisions with optically centrifuged molecules. In 2017 and 2018, increased signal intensities from a multi-pass detection setup enabled studies of $CO_2$ $J = 76$–$100$. The first study highlighted the anisotropic kinetic energy release from collisions and orientational anisotropy values and decay rates that increase as a function of $J$.[23] The second study identified the importance of rotational adiabaticity in collisions of centrifuged $CO_2$ with buffer gases.[24]

The work presented here builds on the previous studies of optically centrifuged $CO_2$ by extending the range of $J$-states up to $J = 282$. For comparison, the rotational energy of the $J = 100$ state is near 3930 $cm^{-1}$ with a downward energy gap of $\Delta E = 150$ $cm^{-1}$, while the energy of the $J = 282$ state is 30 300 $cm^{-1}$ with a comparable energy gap of $\Delta E = 415$ $cm^{-1}$. Our dynamics studies use polarization-sensitive transient IR absorption to characterize the inverted rotational distribution of the centrifuged molecules, their polarization anisotropies, the kinetics of the state-resolved collisional relaxation, and the magnitude of rotation-to-translation energy transfer by measuring Doppler-broadened line profiles.

## II. Methods

The experiments reported here were performed using an optical centrifuge laser system coupled to a high-resolution transient IR absorption spectrometer. The optical centrifuge instrument has been described in detail previously.[1] The key features are presented here and a schematic diagram of the instrumentation is shown in Fig. 1.

The optical centrifuge pulse uses an amplified ultrafast Ti:Sapphire laser system, which generates pulses of light centered at $\lambda = 806$ nm. The pulses are stretched in time from 40 fs to 100 ps and amplified in a regenerative amplifier. The temporal stretching induces a positive chirp. A pulse shaper spectrally splits the original pulses into pairs of pulses, one with $\lambda > 806$ nm denoted $\omega_1$ and the other with $\lambda < 806$ nm denoted $\omega_2$. A negative chirp is induced into $\omega_2$ such that

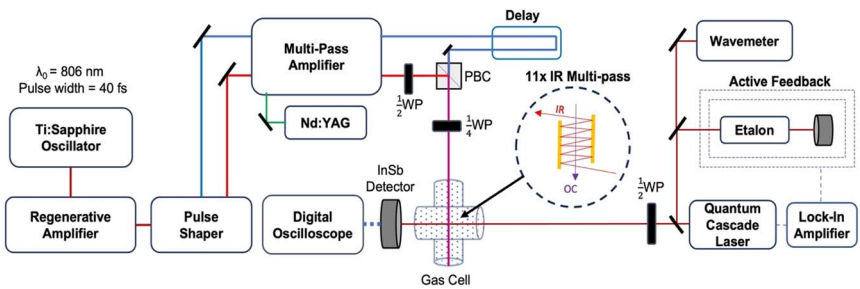


Fig. 1 Schematic diagram of the optical centrifuge and high-resolution transient IR absorption spectrometer. The pair of optical centrifuge pulses have orthogonal linear polarization after the $\frac{1}{2}$-wave plate ($\frac{1}{2}$WP) and opposite circular polarization after the $\frac{1}{4}$-wave plate ($\frac{1}{4}$WP). The IR $\frac{1}{2}$-wave plate is used to control the polarization of the IR probe.

the pair of pulses have an initial wavelength of $\lambda_0 = 806$ nm and their optical frequency difference increases over the time of the pulse. The time-dependent frequency difference is the source of the sequential Raman transitions that lead to optically centrifuged molecules.

The oppositely chirped pulses are sent through a multi-pass amplifier, which is pumped by a 10 Hz Nd:YAG laser at $\lambda = 532$ nm, and are amplified to approximately 20 mJ per pulse each. Once amplified, the pair of pulses is recombined in space with a polarizing beam cube and in time with a delay stage. The recombined pairs of pulses are given opposite circular polarization with a $\frac{1}{4}$-wave plate, resulting in an optical field that angularly accelerates over the pulse duration. Gas-phase $CO_2$ molecules that are trapped in the optical field through an induced-dipole interaction are angularly accelerated into extreme rotational states.

Fig. 2a shows the spectra of the pair of optical centrifuge pulses. The instantaneous angular frequency of the optical centrifuge trap is given by $\Omega_{OC}(t) = \frac{1}{2}(\omega_1(t) - \omega_2(t))$. Fig. 2b shows the intensity profile of the optical trap as a function of $\Omega_{OC}$, based on the intensity profile of $\omega_1(t)$. The extent of rotational excitation in the optically centrifuged molecules is controlled by the spectral bandwidth of the optical centrifuge pulse. Optical centrifuge pulses with the full spectral bandwidth can populate $CO_2$ rotational states near $J = 360$. Here we used reduced bandwidth pulses to preferentially populate rotational states with $J \leq 282$. A tunable optical centrifuge trap is realized by removing a selected short wavelength portion of $\omega_1$ using a micrometer-controlled beam block.

Fig. 2c shows the geometry of the interaction region for the centrifuged molecules. The optical centrifuge propagation vector $\vec{k}_{OC}$ lies along the $z$-axis. Optically centrifuged molecules have unidirectional rotational motion within the $x$–$y$ plane and orientated angular momenta along the $z$-axis. The IR probe beam is propagated along the $x$-axis with vector $\vec{k}_{IR}$. A $\frac{1}{2}$-wave plate controls the polarization of the IR probe, with $\|$-polarization parallel to the $z$-axis ($E_\|$) and $\perp$-polarization ($E_\perp$) perpendicular to the $z$-axis. The optical centrifuge beam is focused to a beam waist of $\omega_0 = 52$ μm. The IR beam is focused to a beam waist of 230 μm.

Individual rotational states of the centrifuged $CO_2$ molecules are measured with high-resolution transient IR absorption spectroscopy from a $\lambda = 4.5$ μm quantum cascade laser (Daylight Solutions). The quantum cascade laser has a resolution of $\Delta\nu \leq 0.0002$ cm$^{-1}$. The IR output frequency is controlled *via* active

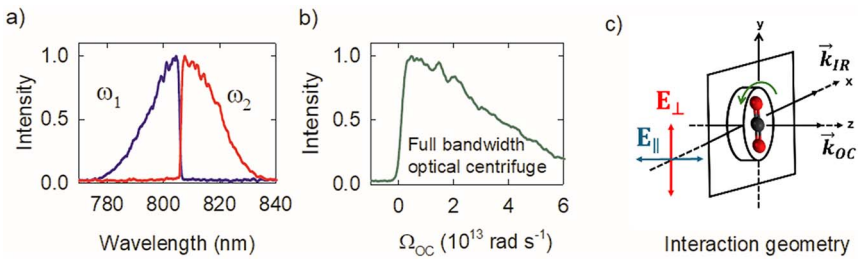


Fig. 2 (a) Spectra of oppositely-chirped optical centrifuge pulses. (b) Profile of the optical centrifuge as a function of angular frequency using the full bandwidth of $\omega_1$. (c) Geometry of the interaction region where optically centrifuged molecules are probed with polarization-sensitive transient IR absorption spectroscopy. The IR polarizations are labeled relative to the $z$-axis.

feedback using a scanning Fabry–Perot etalon and a lock-in amplifier to tune over the $CO_2$ transitions, while the wavelength is monitored on a wavemeter (Bristol Instruments) with a resolution of $\Delta\nu \leq 0.0004$ cm$^{-1}$. Inside the gas cell, the IR beam is overlapped with the optical centrifuge 11 times using an IR multipass (shown in the Fig. 1 inset) to increase signal-to-noise. Spectral features were measured with a 200 ns rise time InSb detector, while dynamics measurements used an InSb detector with a 70 ns rise time. The $CO_2$ pressure used in this experiment is 2.95 Torr based on an equilibrium IR absorption measurement, corresponding to a gas kinetic collision time of ~30 ns. Transient IR measurements at $t = 120$ ns represent $CO_2$ molecules that have undergone approximately four gas-kinetic collisions.

# III. Results and discussion

Here we describe the results of experiments that measure IR transition frequencies for $CO_2$ $(00^01) \leftarrow (00^00)$ R-branch transitions with $J = 186$–$282$ and use those transitions to investigate the collisional relaxation of optically centrifuged molecules with $J = 244$–$282$. We start with a description of line-center transition frequency measurements and compare the results to calculated transition frequencies from the CDSD4000 and predicted frequencies from an expansion of the rigid rotor model. We then use a reduced-bandwidth optical trap to preferentially populate $CO_2$ rotational states with $J \leq 282$.

### a. Transient IR spectroscopy of $CO_2$ $(00^01) \leftarrow (00^00)$ R-branch transitions for $J = 186$–$282$

New IR spectroscopy was needed to investigate the collision dynamics of optically centrifuged $CO_2$. Here, we report 30 new IR R-branch $\nu_3$ fundamental transition frequencies for $CO_2$ with $186 \leq J \leq 282$. An earlier study on the spectroscopy of optically centrifuged $N_2O$ with $140 \leq J \leq 205$ showed that a 3rd order polynomial expansion of the rigid rotor model is a reasonable approach for predicting IR transition frequencies of high-$J$ states of $N_2O$.[26] We started with this approach as a guide to locating high-$J$ $CO_2$ transitions. The predicted high-$J$ transitions are based on a 3rd order polynomial expansion in $J(J + 1)$ of the $(00^00)$ and $(00^01)$ states of $CO_2$ using energies for $J \leq 128$ that is then extrapolated for high-$J$ transitions.[51,52] The expansion is shown in eqn (1).

$$E_{\text{rot}} = BJ(J + 1) - D(J(J + 1))^2 + H(J(J + 1))^3 \quad (1)$$

The fitting parameters used to extrapolate the high-$J$ $CO_2$ rotational energies to high-$J$ are $B_0 = 0.3902$ cm$^{-1}$, $D_0 = 1.3337 \times 10^{-7}$ cm$^{-1}$, and $H_0 = 1.3285 \times 10^{-14}$ cm$^{-1}$ for the $(00^00)$ state, and $B_1 = 0.3871$ cm$^{-1}$, $D_1 = 1.3302 \times 10^{-7}$ cm$^{-1}$, and $H_1 = 1.4176 \times 10^{-14}$ cm$^{-1}$ for the $(00^01)$ state. Differences in the extrapolated energies were used to predict the high-$J$ R-branch transitions. Locating the transitions in this way worked well, but spectral perturbations were observed for transitions with $J > 220$. We then used the effective Hamiltonian calculations in the CDSD4000 to identify transitions in the region of the perturbation.

The optical centrifuge was used to populate $CO_2$ rotational states with $J$ values well above a 300 K distribution and transient IR absorption spectroscopy was used to identify the line center IR transition frequencies. $CO_2$ in the ground vibrational

state has only even $J$ values because of nuclear spin statistics. Line-center transition frequencies ($\nu_{obs}$) were determined by collecting transient absorption signals at discrete IR frequencies in steps of $\delta_\nu \leq 0.003$ cm$^{-1}$. Fig. 3a shows the set of transient absorption signals used to identify the $CO_2$ R282 transition near 2315 cm$^{-1}$. Fig. 3b shows the fractional absorption intensities at $t = 220$ ns after the optical centrifuge pulse as a function of IR frequency. The data are fitted with a Gaussian function and the fit is used to identify the line-center transition frequency. For this transition, line-center frequency is $\nu_{obs} = 2314.9167 \pm 0.003$ cm$^{-1}$. Such scans were collected for the 30 R-branch transitions reported here.

The observed IR R-branch transition frequencies for $J \leq 218$ are within 0.01 cm$^{-1}$ of the frequencies predicted by the 3rd order polynomial expansion in $J(J + 1)$. The predicted values are denoted $\nu_{pred}$. However, starting at R220 and going to R256, the observed transition frequencies deviate exponentially from the predicted values. The observed deviation for the R256 transition is 3.2 cm$^{-1}$. An exponential fit of the spectral deviations predicted a frequency deviation for the R258 transition of 4.43 cm$^{-1}$ but no transition was observed in this spectral region.

To identify the observed deviations for additional transitions, the predicted values from the 3rd order polynomial expansion were compared to transition frequencies from the effective Hamiltonian calculations CDSD4000.[54] The transition frequency differences of $\nu_{calc}$ and $\nu_{pred}$ are presented in Fig. 4a, showing that two spectral perturbations are present in the R-branch transitions near R258 and R292. Using the calculated frequencies as a guide, we observed the R268 to R282 transitions. The R258 to R266 transitions remain elusive, in part because of interference with strongly absorbing ambient $CO_2$ lines. A comparison of the observed transition frequencies relative to the predicted values is shown in Fig. 4b. There is excellent agreement between the observed and calculated transition frequencies. Table 1 lists the transition frequencies measured in this study, along with calculated frequencies, deviations, and rotational energies $E_{rot}$ from the effective Hamiltonian calculations.

To understand the vibrational states responsible for the perturbations, the CDSD4000 ($00^00$) and ($00^01$) energies were fit to a 3rd order polynomial expansion in $J(J + 1)$ with $J \leq 300$.[54] The results were used to predict unperturbed high-$J$

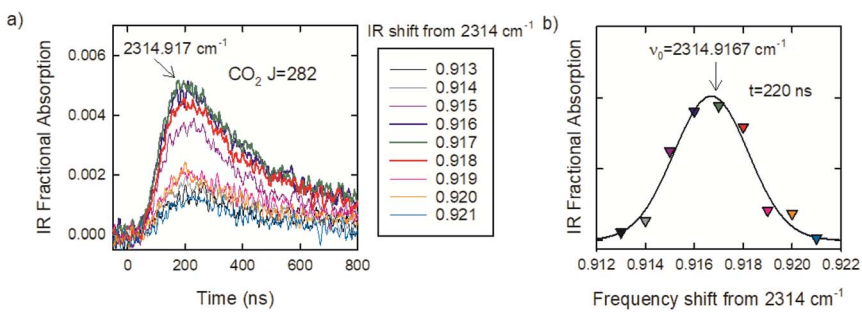


Fig. 3 (a) Transient signals of the $CO_2$ R(282) transition collected as a function of IR frequency. (b) The signals at $t = 220$ ns were fit to a Gaussian (black line) to identify the line-center frequency.

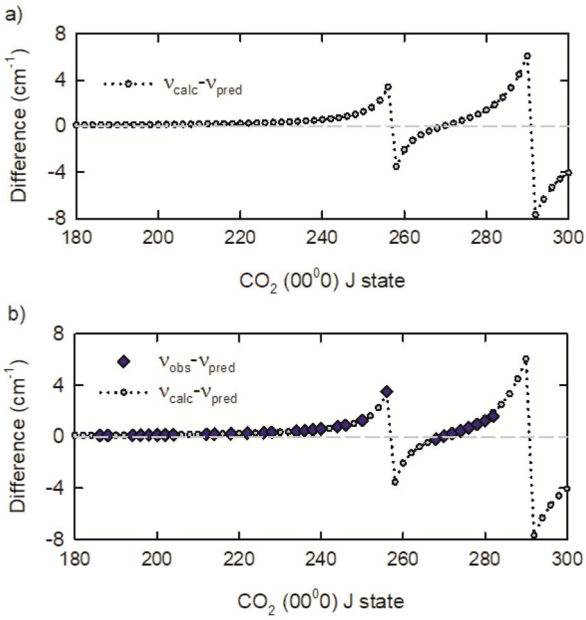


Fig. 4 (a) A comparison of calculated ($v_{calc}$) and predicted ($v_{pred}$) transition frequencies for $CO_2$ R-branch transitions. (b) A comparison of observed transition frequencies $v_{obs}$ with the calculated and predicted values.

energies for both vibrational states. The deviations from the calculated and predicted energies are shown in Fig. 5. The ($00^00$) state of $CO_2$ shows no $J$-dependent structure, but the ($00^01$) state shows distinct energy deviations near $J = 259$ and 293. This comparison shows that the ($00^01$) state is coupled to other $CO_2$ rovibrational states with energies near ($00^01$) $J = 259$ and 293.

The $H_{eff}$ model accounts for three vibrational states of $CO_2$ that interact with the ($00^01$) state.[54] The interacting vibrational states are ($03^30$), ($11^10(1)$), and ($11^10(2)$) where (1) and (2) identify Fermi-mixed states. Based on this model, energy level crossings are present near the $J = 259$ rotational states of the ($00^01$) and ($03^30$) vibrational states and near the $J = 291$ rotational state of the ($00^01$) and ($11^10(1)$) vibrational states. The ($11^10(2)$) state interacts indirectly through the ($03^30$) state. Based on the effective Hamiltonian, the authors identify Fermi, Fermi + L-type, and Coriolis coupling as being responsible for the perturbations. While the perturbations affect the IR transition frequencies, they do not affect the rotational energies of the $CO_2$ ($00^00$) vibrational state, which is the topic of the dynamics measurements described in the next section.

### b. State-resolved collisional relaxation of optically centrifuged $CO_2$ $J = 244$–282

Here, we present results of collisional relaxation experiments of optically centrifuged $CO_2$ molecules with $J = 244$–282, using the IR transitions reported in the previous section. We used polarization-sensitive, high-resolution IR probing to characterize the distribution of the optically centrifuged molecules, their

Table 1 Observed ($\nu_{obs}$) and calculated ($\nu_{calc}$) R-branch transition frequencies for the $CO_2$ $\nu_3$ fundamental ($00^01 \leftarrow 00^00$), their differences, and rotational energies

| $J$ state | $\nu_{obs}$ ($\pm$0.003 cm$^{-1}$) | $\nu_{calc}$[a] (cm$^{-1}$) | $\Delta(\nu_{obs} - \nu_{calc})$ (cm$^{-1}$) | $E_{rot}$[a] (cm$^{-1}$) |
|---|---|---|---|---|
| 186 | 2383.921 | 2383.914 | 0.008 | 13411.817 |
| 188 | 2383.070 | 2383.065 | 0.005 | 13697.486 |
| 194 | 2380.360 | 2380.365 | −0.005 | 14571.852 |
| 196 | 2379.421 | 2379.413 | 0.008 | 14869.078 |
| 198 | 2378.443 | 2378.435 | 0.008 | 15169.181 |
| 200 | 2377.441 | 2377.432 | 0.009 | 15472.156 |
| 202 | 2376.413 | 2376.402 | 0.011 | 15777.998 |
| 204 | 2375.359 | 2375.347 | 0.012 | 16086.702 |
| 212 | 2370.885 | 2370.87 | 0.015 | 17350.035 |
| 214 | 2369.704 | 2369.688 | 0.016 | 17672.972 |
| 218 | 2367.267 | 2367.247 | 0.020 | 18327.332 |
| 222 | 2364.730 | 2364.707 | 0.023 | 18992.972 |
| 226 | 2362.095 | 2362.071 | 0.024 | 19669.847 |
| 228 | 2360.743 | 2360.717 | 0.026 | 20012.485 |
| 234 | 2356.552 | 2356.522 | 0.030 | 21057.125 |
| 236 | 2355.113 | 2355.083 | 0.030 | 21410.896 |
| 238 | 2353.658 | 2353.625 | 0.033 | 21767.435 |
| 240 | 2352.186 | 2352.151 | 0.035 | 22126.738 |
| 244 | 2349.208 | 2349.172 | 0.036 | 22853.609 |
| 246 | 2347.712 | 2347.682 | 0.030 | 23221.164 |
| 250 | 2344.796 | 2344.78 | 0.016 | 23964.486 |
| 256 | 2341.879 | 2341.775 | 0.104 | 25099.903 |
| 268 | 2327.177 | 2327.168 | 0.009 | 27443.674 |
| 270 | 2325.475 | 2325.466 | 0.009 | 27843.681 |
| 272 | 2323.728 | 2323.73 | −0.002 | 28246.351 |
| 274 | 2321.958 | 2321.979 | −0.021 | 28651.677 |
| 276 | 2320.175 | 2320.227 | −0.052 | 29059.651 |
| 278 | 2318.398 | 2318.494 | −0.096 | 29470.268 |
| 280 | 2316.637 | 2316.803 | −0.166 | 29883.520 |
| 282 | 2314.920 | 2315.188 | −0.268 | 30299.400 |

[a] From $H_{eff}$ calculations by Tashkun and Perevalov in the CDSD4000.[54]

orientational properties, and their decay kinetics. For these measurements, the bandwidth of the $\omega_1$ optical pulse was reduced to limit the extent of $CO_2$ rotational excitation to states with $J > 282$, thereby limiting the effect of downward collisions that populate the $J = 244$–$282$ states.

**1. Controlling the rotational distribution with a reduced bandwidth optical centrifuge.** A series of reduced bandwidth optical centrifuge (OC) traps were used to minimize population in $CO_2$ states with $J > 282$. Fig. 6a shows the reduced bandwidth optical trap profiles along with the classical rotational frequency $\Omega_J = 4.15 \times 10^{13}$ rad s$^{-1}$ for $J = 282$. Transient IR absorption signals, such as in Fig. 3a, were collected at line-center for $CO_2$ $J = 282$ as the optical centrifuge bandwidth was sequentially reduced. Fig. 6b shows the transient IR fractional absorption signals at $t = 300$ ns as a function of the relative optical centrifuge intensity at $\Omega_{OC} = \Omega_J$ for $J = 282$. The first reduction in the OC spectral bandwidth leads to a 30% increase in the $J = 282$ population. Further OC bandwidth reductions lead to monotonic decreases in the $J = 282$ population. The collisional relaxation

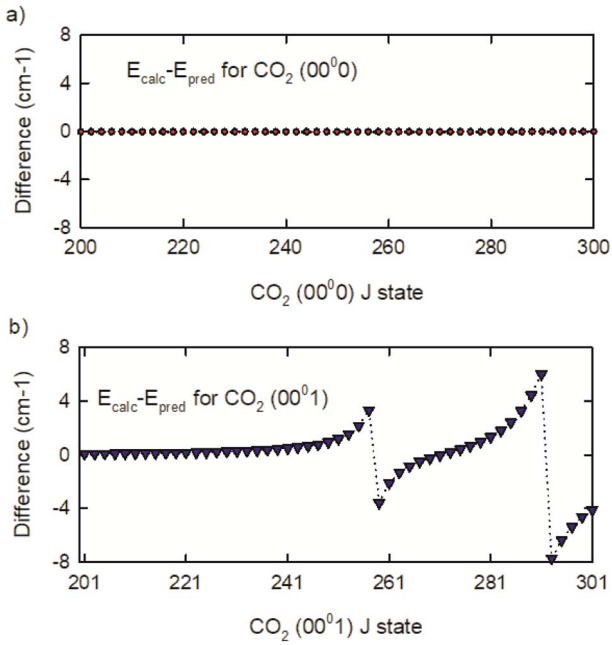


Fig. 5 Differences of calculated and predicted energies for the (a) ($00^00$) and (b) ($00^01$) states of $CO_2$.

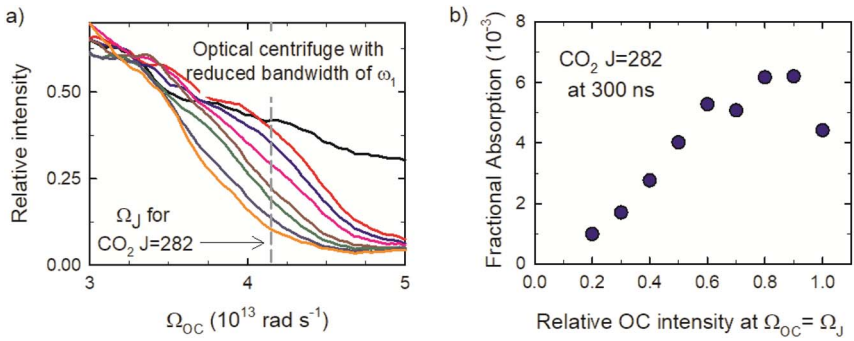


Fig. 6 (a) Optical centrifuge profiles with reduced bandwidth near the classical rotation frequency $\Omega_J$ for $CO_2$ $J = 282$. (b) Transient IR absorption intensities for $J = 282$ at $t = 300$ ns as a function of the optical centrifuge relative intensity at $\Omega_{OC} = \Omega_J$.

studies were performed with the OC intensity reduced to 40% of the full bandwidth intensity at $\Omega_J$. These conditions minimized population in states with $J >$ 282 and resulted in an inverted rotational distribution of centrifuged molecules that has a maximum near $J = 268$.

**2. Polarization measurements of optically centrifuged $CO_2$ in $J = 244$–282.** Time-dependent signals of optically centrifuged $CO_2$ molecules with $J = 244$–282 were measured with polarization-sensitive transient IR absorption probing in the interaction geometry shown in Fig. 2c. Fractional IR absorption intensities with $\|$-polarized light ($I_\|$) and $\perp$-polarized light ($I_\perp$) were used to determine to the

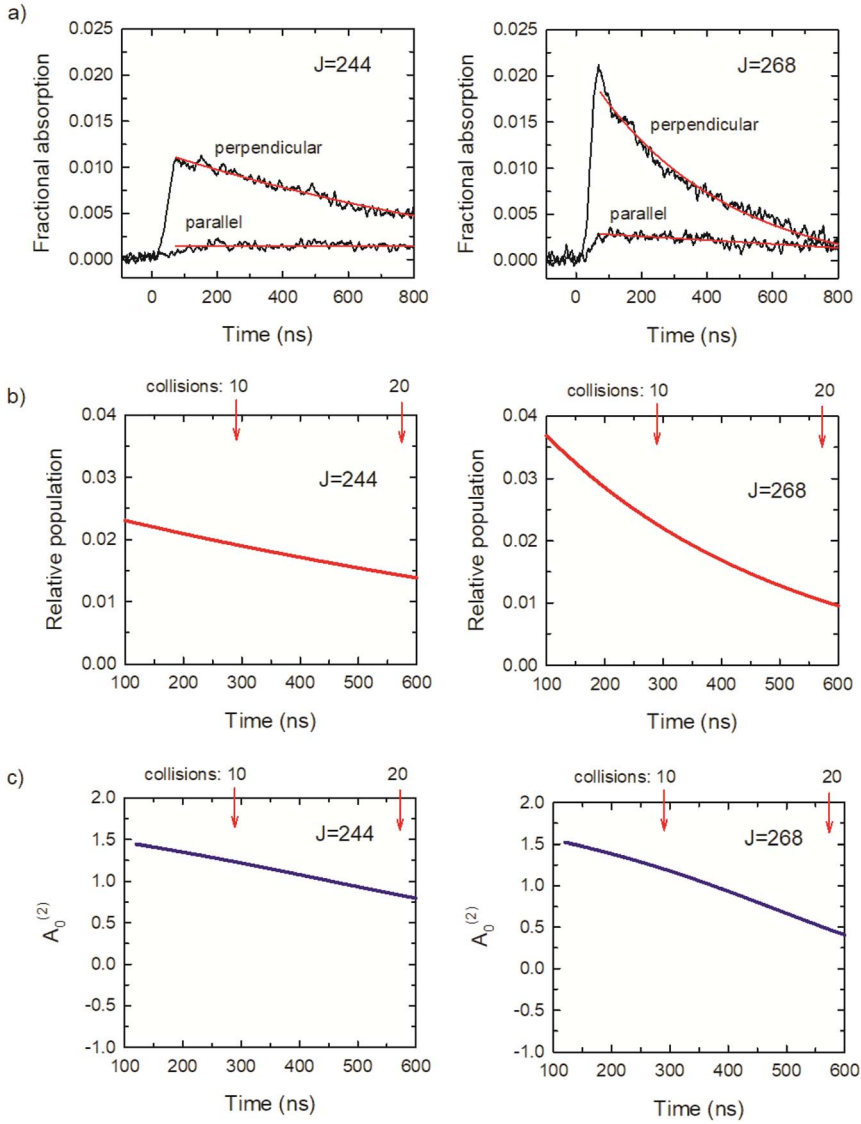


Fig. 7 (a) Polarization-sensitive transient IR absorption signals for optically centrifuged $CO_2$ $J = 244$ and 268. (b) Population for $J = 244$ and 268, showing evidence of a population inversion for the centrifuged molecules. (c) Initial alignment moment values of the centrifuged molecules are near $A_0^{(2)} = 1.5$, showing a high degree of alignment in the $x$–$y$ plane. The average number of collisions is indicated in (b) and (c).

population in individual $J$ states and the alignment in the $x$–$y$ plane. The relative population is given by $2I_\perp + I_\parallel$. The extent of alignment is given by the polarization anisotropy $R = (I_\parallel - I_\perp)/(2I_\perp + I_\parallel)$ and the alignment moment $A_0^{(2)}$.[59–61] For IR probing in the high-$J$ limit with R-branch transitions, the alignment moment is $A_0^{(2)} = -4R$.[62,63] The limits of the alignment moment are $A_0^{(2)} = +2$ for the angular momentum vector $\vec{J}$ parallel to the $z$-axis and $A_0^{(2)} = -1$ for $\vec{J}$ perpendicular to the $z$-axis.

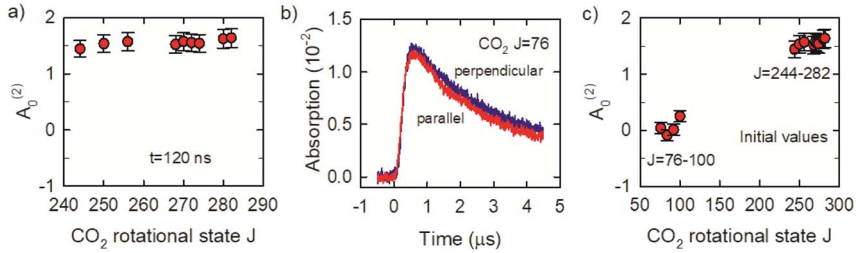


Fig. 8 (a) Alignment moment $A_0^{(2)}$ of optically centrifuged $CO_2$ $J = 244$–$282$ at $t = 120$ ns. (b) Polarization-sensitive transient IR absorption signals for $J = 76$. (c) Comparison of initial $A_0^{(2)}$ values for $CO_2$ $J = 244$–$282$ and $J = 76$–$100$.

Fig. 7a shows transient absorption signals $I_\perp$ and $I_\parallel$ in black for $CO_2$ $J = 244$ and 268. The rise times of the transient signals are detector limited, showing that these states are prepared directly by the optical centrifuge pulse. Approximately 3 collisions having occurred at $t = 100$ ns, based on the average collision time of 29 ns at a pressure of 2.95 Torr. The $\perp$-polarized data from $t = 120$ ns to 1 μs were fit to a 3-parameter exponential decay function, and the $\parallel$-polarized data over the same time range were fit to a linear function. The results are shown in red in Fig. 7a. The fit parameters were used to determine the time-dependent population and alignment values, shown in Fig. 7b and c, based on the expressions above. The optical centrifuge pulses were adjusted to optimize population in the $J = 268$ state. Evidence of the population inversion for the centrifuged molecules is evident with the initial population for $J = 268$ twice that of $J = 244$. The $\perp$-polarized signals are an order of magnitude larger than the $\parallel$-polarized signals, indicating a significant polarization in both states. These features are representative of the transient absorption signals for the $CO_2$ $J = 244$–$282$ states.

We now consider the $J$-dependence of the alignment in the $x$–$y$ plane of optically centrifuged $CO_2$ molecules with $J = 244$–$282$. Fig. 8a shows that the alignment moments at $t = 120$ ns are close to $A_0^{(2)} = 1.5$, indicating a high degree of alignment relative to the excitation polarization of the optical centrifuge. We performed additional measurements for the $CO_2$ $J = 76$–$100$ states to check for evidence of alignment in the collision products. The $J = 76$–$100$ states are not populated directly in the optical centrifuge pulse; instead, they are populated through collisions of optically centrifuged molecules with the thermal bath. Fig. 8b shows the fractional absorption intensities $I_\perp$ and $I_\parallel$ for $J = 76$. These signals have rise times that are 6-fold longer than those for the $J = 244$–$282$ states, consistent with collision-induced population growth. The $I_\perp$ and $I_\parallel$ signals for $J = 76$–$100$ have similar intensities and decay rates. The alignment moment values for these states are close to zero, as shown in Fig. 8c, indicating that the collisions involve a broad range of scattering angles.

**3. Relaxation kinetics of optically centrifuged $CO_2$ $J = 244$–$282$.** Here we consider the time-dependence of the optically centrifuged $CO_2$ molecules in terms of population and anisotropy decay. Generally, collisional relaxation rates for state $J$ include contributions from collisions that move population into $J$ and those that move population out of $J$. Eqn (2) is the state-specific rate expression for $CO_2(J)$ that includes both processes.

$$\frac{d}{dt}[CO_2(J)] = \sum k_{in}^{J'} \left[CO_2(J')\right][M] - k_{out}^{J}[CO_2(J)][M] \quad (2)$$

In eqn (2), $J'$ is any state other than $J$ and $M$ is a collision partner with number density $[M]$ based on the cell pressure. The highest $J$ states prepared in the optical centrifuge relax predominantly by moving to lower rotational states. For the study reported here, there is essentially no population in states with $J > 282$, which reduces the impact of the first term on the right-hand side of eqn (2). It is also unlikely that collisions move population into higher $J$ states because the energy gaps of 370–420 $cm^{-1}$ for the $J = 244$–$282$ states are large compared to the relative collision energy at 300 K. In our analysis, we do not include the first term on the right-hand side of eqn (2). The effect is negligible for $J = 282$, but the apparent decay rates for states further down the collisional cascade are reduced by incoming population and represent lower limits to $k^J_{out}$. The relaxation occurs

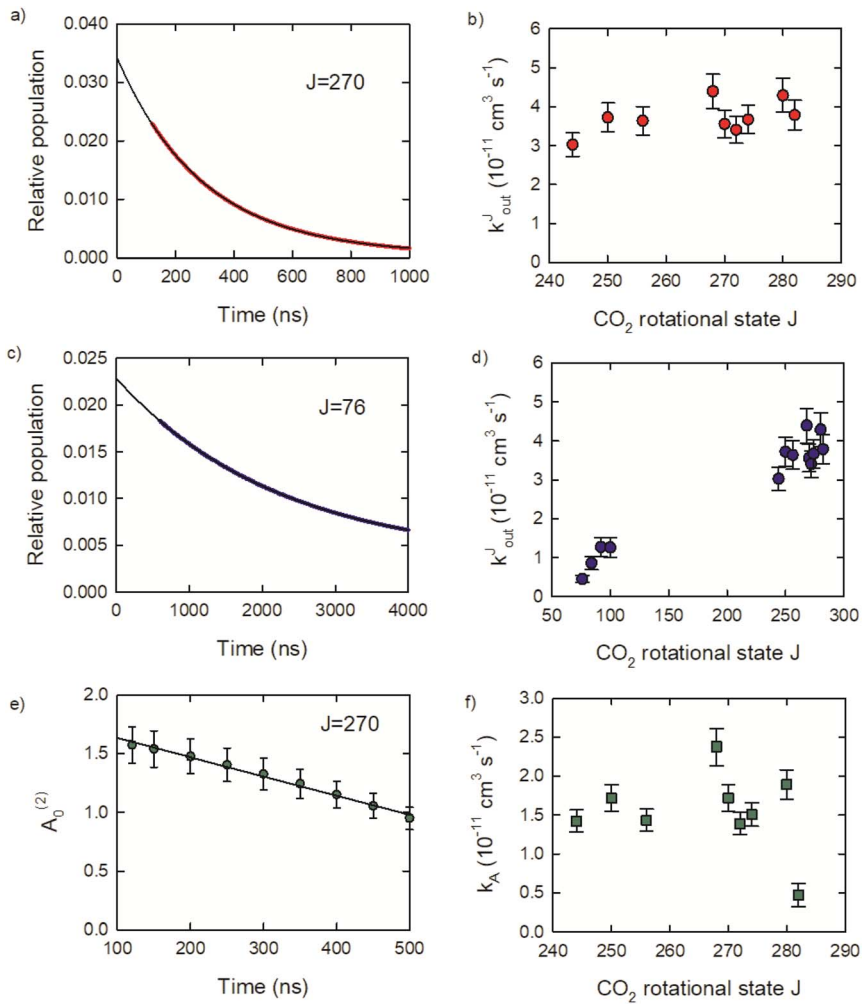


Fig. 9 (a) Population decay curve and fit for $CO_2$ $J = 270$. (b) Relaxation rate constants for $J = 244$–$282$. (c) Population decay curve and fit for $CO_2$ $J = 76$. (d) Inclusion of relaxation rate constant for $J = 76$–$100$. (e) Time-dependent alignment measurements for $J = 270$ and linear fit results. (f) Alignment decay constants for $J = 244$–$282$.

under pseudo-first order conditions, where $[M]$ is approximately constant. Here we define a pseudo-first order rate constant $k \equiv k^J_{out}[M]$. Under these conditions, the population time-dependence is $[CO_2(J)]/[CO_2(J)]_0 = e^{-kt}$.

Relaxation rate constants were determined from decay lifetimes for individual rotational states with $J = 244$–$282$ by fitting the population to exponential decay functions. Fig. 9a shows the population decay (in red) for $J = 270$ along with the fit results in black. The $J$-dependent rate constants for these states are shown in Fig. 9b, with values of $k^J_{out} = (4.3 \pm 0.4) \times 10^{-11}$ cm$^3$ molecule$^{-1}$ s$^{-1}$ for $J = 280$ and $k^J_{out} = (3.0 \pm 0.3) \times 10^{-11}$ cm$^3$ molecule$^{-1}$ s$^{-1}$ for $J = 244$. These rate constants are an order of magnitude smaller than the Lennard-Jones collision rate constant $k_{LJ} = 3.7 \times 10^{-10}$ cm$^3$ molecule$^{-1}$ s$^{-1}$, showing that population loss does not occur on every collision for the $J = 244$–$282$ states.

Relaxation kinetics were also measured for several states with $J = 76$–$100$ to better characterize the overall collisional relaxation. These states are populated by the collisional cascade of the optically centrifuged molecules. The population decay for $J = 76$ is shown (in blue) in Fig. 9c, along with an exponential fit. Fig. 9d shows that the rate constants for $J = 76$, 84, 92 and 100 are significantly smaller than the values for $J = 244$–$282$, consistent with the overall relaxation process.

Without state-to-state cross sections, either from experiments or calculations, it is not possible to assess how the observed relaxation rate constants compare to predicted values from statistical models that have been used for lower $J$ states. At present, the reported rate constants for $CO_2$ relaxation are benchmarks for future studies. In a related study on CO($J$) relaxation, however, we used master equation simulations to calculate the relaxation kinetics and rotational distributions of optically centrifuged CO with $J \leq 80$, based on extrapolated rate constants from state-to-state measurements for $J = 0$–$29$.[27,28] The simulations successfully reproduced the qualitative features of the experimental results, with the key exception that the calculated relaxation rate constants were 5 times larger than those measured in the experiments. The statistical model for the CO system considered the increasing energy gaps for high $J$ states, but the effects of large angular momentum and short rotational periods were not included.

Here we consider the time-dependence of the molecular alignment in the $x$–$y$ plane. The $A_0^{(2)}$ values for $CO_2$ $J = 270$ are shown in Fig. 9e as a function of time. Loss of alignment in the centrifuged molecules occurs through collisions and pseudo-first order kinetics were used to describe the time-evolution of $A_0^{(2)}$, such that $(A_0^{(2)})_t/(A_0^{(2)})_{t=0} = e^{-k_A[M]t}$. The decay profiles are linear for the $J = 244$–$282$ states and rate constants were determined using $(A_0^{(2)})_t/(A_0^{(2)})_{t=0} = -k_A[M]t$.

The resulting $k_A$ values are near $k_A = 2 \times 10^{-11}$ cm$^3$ molecule$^{-1}$ s$^{-1}$ for $J = 244$–$280$. However, $k_A$ for $J = 282$ is four times smaller, with $k_A = 4.7 \times 10^{-12}$ cm$^3$ molecule$^{-1}$ s$^{-1}$. This result shows that while collisions reduce the alignment of the optically centrifuged molecules, the effect is less apparent for the highest populated state. The alignment decay for the $J = 282$ state results from collisions that reorient a subset of molecules originally prepared by the optical centrifuge, but does not include incoming signal from the relaxation of higher $J$ states. There are no $J$ states populated above $J = 282$ and up-collisions from lower $J$ are unlikely given the relatively large energy gaps of 420 cm$^{-1}$ or more. In this way, the $J = 282$ state is unique among the set of states investigated here.

We also find that the alignment decay rates are a factor of two times smaller than the population decay rates. This set of rate constants for population and

 

alignment decay show that collisions of optically centrifuged $CO_2$ are more likely to reduce the $J$ quantum number of the centrifuged molecules than to induce large changes in the $m_J$ projection quantum number (without accompanying changes in $J$) that lead to randomization of their spatial orientations.

**4. Angular momentum projection quantum numbers from anisotropy measurements.** In this section, we use our polarization anisotropy measurements to characterize the average angular momentum projection $m_J$ quantum numbers for optically centrifuged $CO_2$ in $J = 244$–$282$. The alignment moment $A_0^{(2)}$ can be written in terms of the average cosine squared of the angle $\theta$ between $\vec{J}$ and the symmetry axis ($z$), such that

$$A_0^{(2)} = \langle 2P_2(\cos\theta)\rangle = (3\langle\cos^2\theta\rangle - 1), \quad (3)$$

where $P_2(\cos\theta)$ is the second Legendre polynomial as a function of $\cos\theta$.[59–61] The average values of $\cos^2\theta$ were used to determine average $m_J$ quantum numbers for the optically centrifuged molecules using the high-$J$-limiting vector model expression $\cos\theta = m_J/(J(J+1))^{1/2}$. Fig. 10a shows the time evolution of $\langle m_J\rangle$ for the $J = 244$–$282$ states, along with the average number of collisions. The $\langle m_J\rangle$ values at $t = 120$ ns are slightly smaller than $J$ and undergo collision-induced hops to lower $m_J$ levels. Fig. 10b plots $\langle\cos\theta\rangle = m_J/(J(J+1))^{1/2}$ as a function of $J$ at $t = 120$ ns, showing that $\langle m_J\rangle > 0.9\,(J(J+1))^{1/2}$ for this set of states. The $\langle m_J\rangle$ hop rate is defined as the number of $\langle m_J\rangle$ hops per collision and Fig. 10c shows that hop rate is 2–3 hops per collision, on average. It is notable that the $\langle m_J\rangle$ hop rate for $J = 282$ is smaller than for the other $J$ states. $J = 282$ is the highest state in the ensemble of centrifuged molecules and there are no states higher in energy to populate $J = 282$ through collisions. This result is consistent with our observation that $J$-changing collisions occur more readily than collisions that only induce changes in $\langle m_J\rangle$.

**5. Rotation to translation energy transfer of optically centrifuged $CO_2$.** The extent of rotation to translation energy transfer was investigated for optically

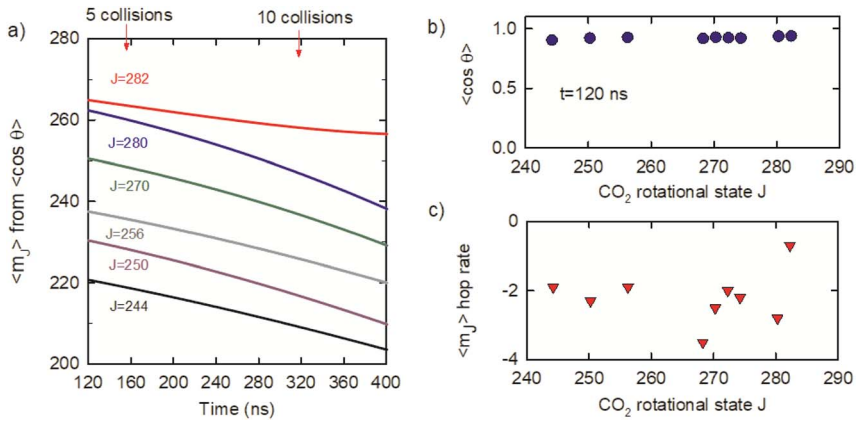


Fig. 10 (a) Average angular momentum projection quantum numbers $m_J$ for optically centrifuged $CO_2$ molecules as a function of time, from polarization anisotropy measurements. (b) $J$-Dependence of $\langle\cos\theta\rangle$ values at $t = 120$ ns illustrates the extent of alignment in the optically centrifuged molecules. (c) Hop rates for $\langle m_J\rangle$ transitions on a per collision basis for different $J$ states, based on the data in (a).

centrifuged $CO_2$ by measuring Doppler-broadened transient IR line profiles. Fig. 11a and b show the Doppler-broadened line profiles for $J = 92$ and $J = 280$ at 200 ns following the optical centrifuge pulse and collected with $E_\perp$ IR light. The symbols are the fractional IR absorption and the Gaussian curves are fits of the data. The translational temperature is determined from the full-width-half maximum of the Gaussian fits. The $J = 92$ state has a translational temperature of $T_{trans} = 1430 \pm 220$ K at 200 ns. For the $J = 280$ state, the translational energy is $T_{trans} = 370 \pm 30$ K at 200 ns.

The Doppler profiles show that collisions of optically centrifuged $CO_2$ molecules with thermal bath molecules are impulsive, leading to rotational excitation of the bath molecules and translational energy in both collision partners. The high degree of alignment of the centrifuged molecules in the $x$–$y$ plane results in collision products that are scattered predominantly outward from the $z$-axis with cylindrical symmetry and the most effective collisions for energy transfer will have relative velocities that are in the $x$–$y$ plane. Doppler profiles measured along the $x$-axis therefore characterize the maximum recoil velocities of the scattered molecules.

The difference in the Doppler broadening for $J = 92$ and $J = 280$ is an indication that the optically centrifuged molecules have lower initial velocities than the thermal bath molecules. Fig. 11c considers the velocity vectors before and after a head-on collision with a $b = 0$ impact parameter, in the lab frame and the center of mass (cm) frame. The lab frame velocities before the collision are $v_1$ for the centrifuged molecule and $v_2$ for the thermal bath molecule; the corresponding cm velocities are $w_1$ and $w_2$. After the collision, the cm velocities $w_3$ (for the centrifuged molecule) and $w_4$ (for the bath molecule) are equal and opposite. However, in the lab frame, $v_3 < v_4$ and the high-$J$ collision products have narrower Doppler profiles.

Previous studies from our laboratory provide additional support that the centrifuged molecules have sub-thermal velocity distributions.[21] In depletion measurements of $CO_2$ following the optical centrifuge pulse, the $J = 0$ and $J = 36$ states have narrow Doppler profiles that correspond to translational temperatures of 130 and 140 K, respectively, showing that a translationally cool set of molecules are centrifuged to higher states. Further translational cooling may also take place during the optical centrifuge pulse through electrostriction in the focused laser beam. This phenomenon will be the focus of future investigations.

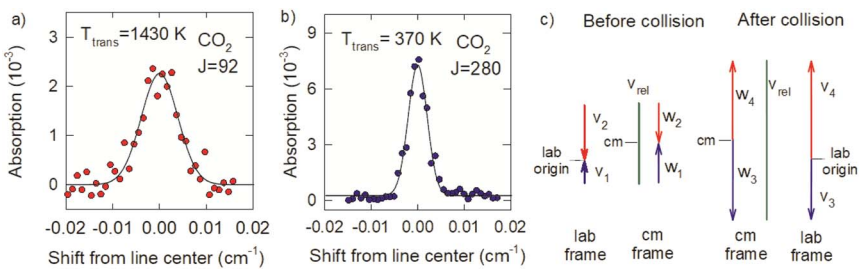


Fig. 11 Doppler-broadened line profiles for $CO_2$ (a) $J = 92$ and (b) $J = 280$ at 200 ns following the optical centrifuge pulse. (c) Velocity vectors in the lab frame ($v$) and center of mass (cm) frame ($w$) for a collision with $b = 0$ of an optically centrifuged molecule and a thermal bath molecule, before (1, 2) and after (3, 4) collisional energy transfer.

# IV. Conclusions

We have investigated the spectroscopy and collision dynamics of optically centrifuged $CO_2$ with rotational states $J \leq 282$ using polarization-sensitive high-resolution transient IR absorption spectroscopy. For these studies, the optical centrifuge laser bandwidth was reduced so that the highest populated rotational state was $J = 282$. New IR fundamental $\nu_3$ R-branch transitions were measured using the optical centrifuge to populate high-$J$ states of $CO_2$. Except in regions of two spectral perturbations, the observed transitions were well predicted by extrapolating from low-$J$ spectral constants of a third-order expansion of the rigid-rotor model.

The nearly nascent distribution of the centrifuged molecules with $J = 244$–$282$ peaks at $J = 268$, and the centrifuged molecules have a high degree of alignment with the initial excitation polarization. The alignment moments for this set of optically centrifuged states are near $A_0^{(2)} = 1.5$, which is near the maximum value of $A_0^{(2)} = 2$. The centrifuged molecules are prepared with average angular momentum projection $m_J$ quantum numbers that are within 90% of the $J$ vector based on measured values of $A_0^{(2)}$. Through collisions, the centrifuged molecules gradually lose their alignment, but the anisotropy decay is slower than the population decay. Collisions lead to rotational excitation of thermal bath molecules, and transient measurements on the $J = 76$–$100$ states show that these collision products have a low degree of alignment.

The results presented here provide a clear picture of the rotation-to-translation energy transfer mechanism for molecules with large amounts of angular momentum. Our results reveal that collisions of centrifuged molecules impart rotational energy to thermal bath molecules, along with translational energy to both collision partners. A comparison of $J$-dependent Doppler profiles indicates that the centrifuged molecules initially have translational energies that are less than the thermal average, showing that the centrifuged molecules are prepared with relatively low kinetic energies. Collisional relaxation rate constants for the $J = 244$–$282$ states are near one-tenth the gas kinetic collision rate constant. Reduced collisional energy transfer rates are associated with increasing rotational energy gaps. Without state-to-state rate information for $CO_2$–$CO_2$ collisions, it is not possible to compare the rate results to statistical models. However, statistical models that work well for low-$J$ CO–CO collisions overestimate the observed relaxation rate constants for high-$J$ molecules, suggesting that angular momentum effects must also be considered. Future studies will take advantage of the tunability in the optical centrifuge to investigate $CO_2$ collisional phenomena over a broader range of rotational states in order to elucidate $J$-dependent behavior in more detail.

These studies demonstrate the power of modern optical methods for generating and investigating molecules with large amount of controllable angular momentum. New IR spectral lines of high-$J$ molecules will contribute to more accurate description of high energy molecules, and enable future investigations of high energy environments and remote atmospheres. The results reported here contribute to a growing body of work that highlight the impact of large amounts of angular momentum on collisional energy transfer, and the underlying principles that control molecular collisions.

## Author contributions

Investigation: M. E. Ritter, S. A. DeSouza, H. M. Ogden, T. J. Michael, and A. S. Mullin; conceptualization: M. E. Ritter, S. A. DeSouza, H. M. Ogden, and A. S. Mullin; methodology: H. M. Ogden, and A. S. Mullin; formal analysis: M. E. Ritter, S. A. DeSouza, and A. S. Mullin; project administration and funding acquisition: A. S. Mullin; writing: M. E. Ritter, S. A. DeSouza, H. M. Ogden, and A. S. Mullin.

## Conflicts of interest

There are no conflicts to declare.

## Acknowledgements

The authors gratefully acknowledge Dr Valerii Perevalov for providing helpful insights to the observed spectral perturbation, Dr M. H. Alexander, P. J. Dagdigian, and J. T. Fourkas for provocative discussions on scattering dynamics, and Dr Kenneth G. McKendrick for his informative suggestions. The authors acknowledge research support from the US National Science Foundation through grants CHE-1800531 and CHE-2155135 and the University of Maryland.

## References

1 D. Bailly, C. Camy-Peyret and R. Lanquetin, *J. Mol. Spectrosc.*, 1997, **182**, 10–17.
2 S. Hay, F. Shokoohi, S. Callister and C. Wittig, *Chem. Phys. Lett.*, 1985, **118**, 6–11.
3 A. S. Mullin, J. Park, J. Z. Chou, G. W. Flynn and R. E. Weston, *Chem. Phys.*, 1993, **175**, 53–70.
4 R. Aures, K.-H. Gericke, M. Kawasaki, C. Maul, Y. Nakano, G. Trott-Kriegeskorte and Z. Y. Wang, *PhysChemComm*, 2001, **4**, 102–105, DOI: 10.1039/b108052k.
5 J. Bailey, V. S. Meadows, S. Chamberlain and D. Crisp, *Icarus*, 2008, **197**, 247–259.
6 Q. Binauld, P. Rivière and A. Soufiani, *Combust. Flame*, 2018, **194**, 128–134.
7 M. R. Swain, G. Tinetti, G. Vasisht, P. Deroo, C. Griffith, J. Bouwman, P. Chen, Y. Yung, A. Burrows, L. R. Brown, J. Matthews, J. F. Rowe, R. Kuschnig and D. Angerhausen, *Astrophys. J.*, 2009, **704**, 1616–1621.
8 G. Tinetti, P. Deroo, M. R. Swain, C. A. Griffith, G. Vasisht, L. R. Brown, C. Burke and P. McCullough, *Astrophys. J. Lett.*, 2010, **712**, L139–L142.
9 J. T. Yardley, *Introduction to Molecular Energy Transfer*, Academic Press, 1980.
10 Y. Ohshima and H. Hasegawa, *Int. Rev. Phys. Chem.*, 2010, **29**, 619–663.
11 G. Karras, M. Ndong, E. Hertz, D. Sugny, F. Billard, B. Lavorel and O. Faucher, *Phys. Rev. Lett.*, 2015, **114**, 103001.
12 O. Korech, U. Steinitz, R. J. Gordon, I. S. Averbukh and Y. Prior, *Nat. Photonics*, 2013, **7**, 711–714.
13 K. Kitano, H. Hasegawa and Y. Ohshima, *Phys. Rev. Lett.*, 2009, **103**, 223002.
14 C. Bloomquist, S. Zhdanovich, A. A. Milner and V. Milner, *Phys. Rev. A*, 2012, **86**, 063413.
15 M. Bitter and V. Milner, *Phys. Rev. A*, 2016, **93**, 013420.

16 J. Karczmarek, J. Wright, P. Corkum and M. Ivanov, *Phys. Rev. Lett.*, 1999, **82**, 3420–3423.
17 D. M. Villeneuve, S. A. Aseyev, P. Dietrich, M. Spanner, M. Y. Ivanov and P. B. Corkum, *Phys. Rev. Lett.*, 2000, **85**, 542–545.
18 L. W. Yuan, S. W. Teitelbaum, A. Robinson and A. S. Mullin, *Proc. Natl. Acad. Sci. U. S. A.*, 2011, **108**, 6872–6877.
19 L. W. Yuan, C. Toro, M. Bell and A. S. Mullin, *Faraday Discuss.*, 2011, **150**, 101–111.
20 C. Toro, Q. N. Liu, G. O. Echebiri and A. S. Mullin, *Mol. Phys.*, 2013, **111**, 1892–1901.
21 M. J. Murray, H. M. Ogden, C. Toro, Q. N. Liu, D. A. Burns, M. H. Alexander and A. S. Mullin, *J. Phys. Chem. A*, 2015, **119**, 12471–12479.
22 M. J. Murray, H. M. Ogden, C. Toro, Q. N. Liu and A. S. Mullin, *ChemPhysChem*, 2016, **17**, 3692–3700.
23 M. J. Murray, H. M. Ogden and A. S. Mullin, *J. Chem. Phys.*, 2017, **147**, 154309.
24 M. J. Murray, H. M. Ogden and A. S. Mullin, *J. Chem. Phys.*, 2018, **148**, 084310.
25 H. M. Ogden, T. J. Michael, M. J. Murray, Q. N. Liu, C. Toro and A. S. Mullin, *Phys. Chem. Chem. Phys.*, 2019, **21**, 14103–14110.
26 H. Ogden, T. Michael, M. Murray and A. Mullin, *J. Quant. Spectrosc. Radiat. Transfer*, 2020, **246**, 106867.
27 T. J. Michael, H. M. Ogden and A. S. Mullin, *J. Chem. Phys.*, 2021, **154**, 134307.
28 M. R. Laskowski, T. J. Michael, H. M. Ogden, M. H. Alexander and A. S. Mullin, *Faraday Discuss.*, 2022, **238**, 87–102.
29 A. Korobenko, A. A. Milner, J. W. Hepburn and V. Milner, *Phys. Chem. Chem. Phys.*, 2014, **16**, 4071–4076.
30 A. Korobenko, A. A. Milner and V. Milner, *Phys. Rev. Lett.*, 2014, **112**, 113004.
31 A. A. Milner, A. Korobenko, J. W. Hepburn and V. Milner, *Phys. Rev. Lett.*, 2014, **113**, 043005.
32 A. A. Milner, A. Korobenko and V. Milner, *New J. Phys.*, 2014, **16**, 093038.
33 A. Korobenko, J. W. Hepburn and V. Milner, *Phys. Chem. Chem. Phys.*, 2015, **17**, 951–956.
34 A. Korobenko and V. Milner, *J. Phys. B: At., Mol. Opt. Phys.*, 2015, **48**, 164004.
35 A. A. Milner, A. Korobenko, J. Floss, I. S. Averbukh and V. Milner, *Phys. Rev. Lett.*, 2015, **115**, 033005.
36 A. A. Milner, A. Korobenko and V. Milner, *Opt. Express*, 2015, **23**, 8603–8608.
37 A. A. Milner, A. Korobenko, K. Rezaiezadeh and V. Milner, *Phys. Rev. X*, 2015, **5**, 031041.
38 A. Korobenko and V. Milner, *Phys. Rev. Lett.*, 2016, **116**, 183001.
39 A. A. Milner, A. Korobenko and V. Milner, *Phys. Rev. A*, 2016, **93**, 053408.
40 V. Milner and J. W. Hepburn, in *Advances in Chemical Physics*, ed. P. Brumer, S. A. Rice and A. R. Dinner, Wiley-Blackwell, Malden, 2016, vol. 159, pp. 395–412.
41 A. A. Milner, A. Korobenko, J. W. Hepburn and V. Milner, *J. Chem. Phys.*, 2017, **147**, 124202.
42 J. Floss, C. Boulet, J.-M. Hartmann, A. A. Milner and V. Milner, *Phys. Rev. A*, 2018, **98**, 043401.
43 A. A. Milner, J. A. M. Fordyce, I. MacPhail-Bartley, W. Wasserman, V. Milner, I. Tutunnikov and I. S. Averbukh, *Phys. Rev. Lett.*, 2019, **122**, 223201.
44 I. MacPhail-Bartley, W. W. Wasserman, A. A. Milner and V. Milner, *Rev. Sci. Instrum.*, 2020, **91**, 045122.

45 I. Tutunnikov, J. Floss, E. Gershnabel, P. Brumer, I. S. Averbukh, A. A. Milner and V. Milner, *Phys. Rev. A*, 2020, **101**, 021403(R).
46 P. Amani, A. A. Milner and V. Milner, *J. Chem. Phys.*, 2021, **155**, 124201.
47 A. A. Milner and V. Milner, *Phys. Rev. A*, 2021, **103**, L041103.
48 A. A. Milner, U. Steinitz, I. S. Averbukh and V. Milner, *Phys. Rev. Lett.*, 2021, **127**, 073901.
49 I. Tutunnikov, U. Steinitz, E. Gershnabel, J.-M. Hartmann, A. A. Milner, V. Milner and I. S. Averbukh, *Phys. Rev. Res.*, 2022, **4**, 013212.
50 T. Y. Chen, S. A. Steinmetz, B. D. Patterson, A. W. Jasper and C. J. Kliewer, *Nat. Commun.*, 2023, **14**, 3227.
51 S. A. Tashkun, V. I. Perevalov, R. R. Gamache and J. Lamouroux, *J. Quant. Spectrosc. Radiat. Transfer*, 2015, **152**, 45–73.
52 I. E. Gordon, L. S. Rothman, C. Hill, R. V. Kochanov, Y. Tan, P. F. Bernath, M. Birk, V. Boudon, A. Campargue, K. V. Chance, B. J. Drouin, J. M. Flaud, R. R. Gamache, J. T. Hodges, D. Jacquemart, V. I. Perevalov, A. Perrin, K. P. Shine, M. A. H. Smith, J. Tennyson, G. C. Toon, H. Tran, V. G. Tyuterev, A. Barbe, A. G. Császár, V. M. Devi, T. Furtenbacher, J. J. Harrison, J. M. Hartmann, A. Jolly, T. J. Johnson, T. Karman, I. Kleiner, A. A. Kyuberis, J. Loos, O. M. Lyulin, S. T. Massie, S. N. Mikhailenko, N. Moazzen-Ahmadi, H. S. P. Müller, O. V. Naumenko, A. V. Nikitin, O. L. Polyansky, M. Rey, M. Rotger, S. W. Sharpe, K. Sung, E. Starikova, S. A. Tashkun, J. Vander Auwera, G. Wagner, J. Wilzewski, P. Wcislo, S. Yu and E. J. Zak, *J. Quant. Spectrosc. Radiat. Transfer*, 2017, **203**, 3–69.
53 L. S. Rothman, I. E. Gordon, R. J. Barber, H. Dothe, R. R. Gamache, A. Goldman, V. I. Perevalov, S. A. Tashkun and J. Tennyson, *J. Quant. Spectrosc. Radiat. Transfer*, 2010, **111**, 2139–2150.
54 S. A. Tashkun and V. I. Perevalov, *J. Quant. Spectrosc. Radiat. Transfer*, 2011, **112**, 1403–1410.
55 M. Paulec, M. Marciniak, K. Gross and D. Azevedo, *Proc. SPIE*, 2018, **10644**, 2303982.
56 G. Tinetti, P. Drossart, P. Eccleston, P. Hartogh, A. Heske, J. Leconte, G. Micela, M. Ollivier, G. Pilbratt, L. Puig, D. Turrini, B. Vandenbussche, P. Wolkenberg, J. P. Beaulieu, L. A. Buchave, M. Ferus, M. Griffin, M. Guedel, K. Justtanont, P. O. Lagage, P. Machado, G. Malaguti, M. Min, H. U. Norgaard-Nielsen, M. Rataj, T. Ray, I. Ribas, M. Swain, R. Szabo, S. Werner, J. Barstow, M. Burleigh, J. Cho, V. C. du Foresto, A. Coustenis, L. Decin, T. Encrenaz, M. Galand, M. Gillon, R. Helled, J. C. Morales, A. G. Muñoz, A. Moneti, I. Pagano, E. Pascale, G. Piccioni, D. Pinfield, S. Sarkar, F. Selsis, J. Tennyson, A. Triaud, O. Venot, I. Waldmann, D. Waltham, G. Wright, J. Amiaux, J. L. Auguères, M. Berthé, N. Bezawada, G. Bishop, N. Bowles, D. Coffey, J. Colomé, M. Crook, P. E. Crouzet, V. Da Peppo, I. E. Sanz, M. Focardi, M. Frericks, T. Hunt, R. Kohley, K. Middleton, G. Morgante, R. Ottensamer, E. Pace, C. Pearson, R. Stamper, K. Symonds, M. Rengel, E. Renotte, P. Ade, L. Affer, C. Alard, N. Allard, F. Altieri, Y. André, C. Arena, I. Argyriou, A. Aylward, C. Baccani, G. Bakos, M. Banaszkiewicz, M. Barlow, V. Batista, G. Bellucci, S. Benatti, P. Bernardi, B. Bézard, M. Blecka, E. Bolmont, B. Bonfond, R. Bonito, A. S. Bonomo, J. R. Brucato, A. S. Brun, I. Bryson, W. Bujwan, S. Casewell, B. Charnay, C. C. Pestellini, G. Chen, A. Ciaravella, R. Claudi, R. Clédassou, M. Damasso, M. Damiano,

C. Danielski, P. Deroo, A. M. Di Giorgio, C. Dominik, V. Doublier, S. Doyle, R. Doyon, B. Drummond, B. Duong, S. Eales, B. Edwards, M. Farina, E. Flaccomio, L. Fletcher, F. Forget, S. Fossey, M. Fränz, Y. Fujii, A. García-Piquer, W. Gear, H. Geoffray, J. C. Gérard, L. Gesa, H. Gomez, R. Graczyk, C. Griffith, D. Grodent, M. G. Guarcello, J. Gustin, K. Hamano, P. Hargrave, Y. Hello, K. Heng, E. Herrero, A. Hornstrup, B. Hubert, S. Ida, M. Ikoma, N. Iro, P. Irwin, C. Jarchow, J. Jaubert, H. Jones, Q. Julien, S. Kameda, F. Kerschbaum, P. Kervella, T. Koskinen, M. Krijger, N. Krupp, M. Lafarga, F. Landini, E. Lellouch, G. Leto, A. Luntzer, T. Rank-Lüftinger, A. Maggio, J. Maldonado, J. P. Maillard, U. Mall, J. B. Marquette, S. Mathis, P. Maxted, T. Matsuo, A. Medvedev, Y. Miguel, V. Minier, G. Morello, A. Mura, N. Narita, V. Nascimbeni, N. Nguyen Tong, V. Noce, F. Oliva, E. Palle, P. Palmer, M. Pancrazzi, A. Papageorgiou, V. Parmentier, M. Perger, A. Petralia, S. Pezzuto, R. Pierrehumbert, I. Pillitteri, G. Piotto, G. Pisano, L. Prisinzano, A. Radioti, J. M. Réess, L. Rezac, M. Rocchetto, A. Rosich, N. Sanna, A. Santerne, G. Savini, G. Scandariato, B. Sicardy, C. Sierra, G. Sindoni, K. Skup, I. Snellen, M. Sobiecki, L. Soret, A. Sozzetti, A. Stiepen, A. Strugarek, J. Taylor, W. Taylor, L. Terenzi, M. Tessenyi, A. Tsiaras, C. Tucker, D. Valencia, G. Vasisht, A. Vazan, F. Vilardell, S. Vinatier, S. Viti, R. Waters, P. Wawer, A. Wawrzaszek, A. Whitworth, Y. L. Yung, S. N. Yurchenko, M. R. Z. Osorio, R. Zellem, T. Zingales and F. Zwart, *Exp. Astron.*, 2018, **46**, 135–209.

57 V. Wilquet, A. Mahieux, A. C. Vandaele, V. I. Perevalov, S. A. Tashkun, A. Fedorova, O. Korablev, F. Montmessin, R. Dahoo and J. L. Bertaux, *J. Quant. Spectrosc. Radiat. Transfer*, 2008, **109**, 895–905.

58 X. C. Huang, R. S. Freedman, S. Tashkun, D. W. Schwenke and T. J. Lee, *J. Mol. Spectrosc.*, 2023, **392**, 111748.

59 R. N. Zare, *Angular Momentum: Understanding Spatial Aspects in Chemistry and Physics*, Wiley-Interscience, 1988.

60 J. R. Lakowicz, *Principles of Fluorescence Spectroscopy*, Kluwer Academic/Plenum Publishers, 2nd edn, 1999.

61 U. Fano and J. H. Macek, *Rev. Mod. Phys.*, 1973, **45**, 553.

62 S. J. McGurk, K. G. McKendrick, M. L. Costen, D. I. G. Bennett, J. Klos, M. H. Alexander and P. J. Dagdigian, *J. Chem. Phys.*, 2012, **136**, 164306.

63 R. Uberna, R. D. Hinchliffe and J. I. Cline, *J. Chem. Phys.*, 1995, **103**, 7934–7945.